

# Adaptive detection method of infrared small target based on target-background separation via robust principal component analysis

Chuanyun Wang <sup>a,b,\*</sup>, Shiyin Qin <sup>a</sup>

<sup>a</sup> School of Automation Science and Electrical Engineering, Beihang University, Beijing 100191, China

<sup>b</sup> College of Computer Science, Shenyang Aerospace University, Shenyang 110136, China



## HIGHLIGHTS

- A target-background separation model (T-BS) is designed.
- An image patch set is generated by using multi-scale transform and patch transform.
- Adaptive weighting parameter is regulated to recover low-rank and sparse matrices.
- A new infrared small target detection method is presented based on T-BS.

## ARTICLE INFO

### Article history:

Received 16 October 2014

Available online 21 January 2015

### Keywords:

Infrared small target detection

Target-background separation

Robust principal component analysis

Adaptive weighting parameter

## ABSTRACT

Motivated by the robust principal component analysis, infrared small target image is regarded as low-rank background matrix corrupted by sparse target and noise matrices, thus a new target-background separation model is designed, subsequently, an adaptive detection method of infrared small target is presented. Firstly, multi-scale transform and patch transform are used to generate an image patch set for infrared small target detection; secondly, target-background separation of each patch is achieved by recovering the low-rank and sparse matrices using adaptive weighting parameter; thirdly, the image reconstruction and fusion are carried out to obtain the entire separated background and target images; finally, the infrared small target detection is realized by threshold segmentation of template matching similarity measurement. In order to validate the performance of the proposed method, three experiments: target-background separation, background clutter suppression and infrared small target detection, are performed over different clutter background with real infrared small targets in single-frame or sequence images. A series of experiment results demonstrate that the proposed method can not only suppress background clutter effectively even if with strong noise interference but also detect targets accurately with low false alarm rate.

© 2015 Elsevier B.V. All rights reserved.

## 1. Introduction

Infrared target detection plays an important role in many areas, such as infrared search and track (IRST), forward looking infrared system (FLIR), space-based infrared system (SBIRS), space tracking and surveillance systems (STSS), early-warning systems, and missile tracking systems [1,2]. However, all these applications require to detect target as early as possible, the size of target is often with only a few pixels because of long imaging distance. On the other

hand, due to the atmospheric refraction, dispersion and absorption, the infrared target radiation energy received by imaging sensor is very low and with dim spotlike feature. Consequently, the infrared small target immersed in complex clutter background is often provided with low signal-to-clutter ratio (SCR), and without concrete shape or texture information [1,3]. Therefore, infrared small target detection is a significant issue with high challenges.

Over the past few decades, many researchers have paid attention to the infrared small target detection, and many detection methods have been presented. The leading methods for this problem can be generally categorized into two groups: the sequence detection methods and the single-frame detection methods. The sequence detection methods fully utilize the spatial and temporal

\* Corresponding author at: School of Automation Science and Electrical Engineering, Beihang University, Beijing 100191, China. Tel.: +86 15811366220.

E-mail address: [wangcy0301@buaa.edu.cn](mailto:wangcy0301@buaa.edu.cn) (C. Wang).

information acquired by imaging sensor and perform preferable effect in many practical applications. However, the detected target or imaging sensor is moving fast in many other applications. The moving induces some serious effects from changes of scene between background and target. As a result, the sequence detection methods would not play well advantages. Moreover, infrared small target detection usually requires fast detection speed and short response time, so the single-frame detection methods could better satisfy this demand. In addition, the single-frame detection methods could be employed in pre-processing of sequence detection methods to reduce complexity [4]. With these considerations in mind, what is more effective and feasible approach to the infrared small target detection in single-frame is still an open issue.

Motivated by the robust principal component analysis, in which a data matrix is the superposition of a low-rank component and a sparse component [5], we suppose the infrared background image is a low-rank matrix, and infrared target and noise images are sparse matrices. By recovering the low-rank and sparse matrices, the target-background separation in infrared small target images could be modeled as an optimization problem. Consequently, the infrared small target detection in single-frame is accomplished by numerical resolving an optimizing decision.

The remainder of this paper is organized as follows: related works are reviewed in Section 2. Section 3 introduces our new target-background separation model. In Section 4, the proposed adaptive detection method of infrared small target is presented in detail. Some experiment results and performance evaluations are explained in Section 5. Finally, the whole paper is concluded with some discussions in Section 6.

## 2. Related works

Conventional infrared small target detection methods concentrate on background clutter suppression based on direct spatial filtering or background estimation methods. Due to the simplicity and performance advantages, some typical filtering methods such as Local Means Remove (LMR) [6], Max-mean and max-median (MMed) [7], and morphological filtering (Top-hat) [8] are widely used to reduce the background clutter, and many new spatial filtering methods have been presented [9–12]. Background estimation methods could detect targets by subtracting the estimated background from original image [13], and spatial filters could be used to estimate the background image [14–17]; Wavelet transform was also adopted to decompose the original image to extract multi-scale and multi-direction detail features, and then the predicted background image could be obtained by separation or reconstruction [18–20].

From another standpoint, target occupies only a few pixels, as well as no shape and texture, could be utilized to measure the similarity between true targets and candidate targets. Template matching technique has been extensively studied and used in pattern recognition application, and some template matching methods for infrared small detection based on normalized cross-correlation was presented [21,22]. In addition, principal component analysis (PCA) can reduce redundancies in high dimensional by using low dimensional linear subspace, the projection coefficients templates obtained from principal component analysis (PCA) and the nonlinear correlation similarity measurement were proposed for template matching [23,24]. Meanwhile, according to the principle of point spread function (PSF), small target training sample images were generated and extracted by principal component analysis (PCA) [25], probabilistic principal component analysis (PPCA) [26], nonlinear principal component analysis (NLPCA) [27] and kernel principal component analysis (KPCA) [28] to establish the principal component subspace, and the similarity between

original image block and reconstructed one could indicate it is a true target or not.

Furthermore, target-background contrast information has received significant attention in many other infrared small target detection methods. Motivated by human visual system (HVS), many researchers have paid attention to simulate the mechanisms of HVS for small target detection. Based on the robust properties of HVS, such as contrast mechanism, multi-resolution representation, size adaptation and pop-out phenomena, a mathematical method achieved target signal enhancement and background clutter suppression simultaneously was presented by maximizing the signal-to-clutter ratio (SCR) in Laplacian scale-space [29,30]. As an important characteristic of HVS, visual attention mechanism was researched to determine the suspicious target regions by computing saliency map using Difference of Gaussians (DoG) filters [31,32]. HVS perceived target brightness according to the contrast between target and background, so researchers exploited Laplacian of Gaussian (LoG) filter or local contrast measure (LCM) to suppress the background clutter and enhance the target intensity simultaneously inspired by the contrast mechanism of HVS [2,3]. Subsequently, the improved LCM (ILCM) was proposed to improve detection rate and reduce false alarm rate, as well as the HVS size-adaptation process and attention shift mechanism are adopted in pre-detection stage and threshold operation with traversal mechanism [33]. Meanwhile, small target detecting and tracking method combining the three mechanisms: contrast mechanism, visual attention and eye movement, was presented, in which DoG filters, Gaussian window and Proportional–Integral–Derivative (PID) were used to simulate the three mechanisms, respectively [34].

Recently, infrared small target detection methods using matrix decomposition were proposed. By low-rank and sparse matrix decomposition, the sparse target component could be separated from infrared image, and the augmented Lagrange method was used to for solving robust principal component analysis (RPCA) [35]. Based on a new infrared patch-image model generated by local patch construction, small target detection task was transformed into an optimization problem of recovering low-rank and sparse matrices [4]. In view of time-consuming problem in nuclear-norm minimization using singular value decomposition, Sobolev norm was introduced to replace the nuclear-norm, and then a small target detection method based on harmonic and sparse matrix decomposition was presented [36]. Motivated by cat-eye effect target identification using compressed sensing, a compressive low-rank and sparse decomposition method for detecting infrared small target was presented, in which the constant  $r$  and  $K$  denote the low-rank of background and sparse of target, respectively, and then Walsh Hadamard matrix was chosen as the measurement matrix [37]. Moreover, a model of low rank and sparse representation (LRSR) based on two over-complete dictionary, which were used to describe the collection data and represent the small target, was presented, and then the small target detection was transformed into separation process of background, noise and target components by solving LRSR [38].

## 3. Target-background separation model

### 3.1. Characteristic of infrared small target images

As the application areas of this research, both airborne IRST and FLIR acquire infrared image by imaging system that sense infrared radiation. Their interest targets are usually aircraft, missile, etc. In view of three major infrared atmospheric window ( $1\text{--}2.7\ \mu\text{m}$ ,  $3\text{--}5\ \mu\text{m}$  and  $8\text{--}14\ \mu\text{m}$ ), the current thermal imaging cameras have two basic infrared wavelength ranges: medium-wave infrared

(3–5 μm) and long-wave infrared (8–12 μm). These conditions are applicable to detect aircraft with medium-wave infrared radiation characteristic of smoke plume and long-wave infrared radiation characteristic of aircraft skin when it is flying with high-speed. Nevertheless, the displayed images in the form of visible light include not only interested target but also background and noise. The infrared radiation characteristic of sky background is related to time, space and climate. The radiation comes from two major parts: diffuse solar radiation (<3 μm) and atmospheric thermal radiation (>4 μm).

**Fig. 1** shows one frame infrared small target image with heavy cloud clutter, and two marked rectangular as local regions of background and target are enlarged for analysis. It is easy to observe that the background occupies the most area of infrared small target image, and the target appears on one or more local small regions and noise affects some pixels randomly. The local region of background presents slowly transitional characteristics, and appears very smooth, continuous and isotropy with good correlation between neighbor pixels, which is low-rank if the image is regarded as a matrix. On the contrary, the local region of target looks like singular point with anisotropy and bad correlation between around neighbor pixels, which is sparse if the image is regarded as a matrix. The difference between background and target by three-dimensional (3-D) mesh surfaces could be easily distinguished.

The continuous acquisition of infrared imaging system in a period of time would generate a sequence of images. Thus, one frame infrared small target image can be formulated as follows:

$$I(x, y, k) = I_b(x, y, k) + I_t(x, y, k) + I_n(x, y, k) \quad (1)$$

where  $I$ ,  $I_b$ ,  $I_t$ ,  $I_n$  represent original image, background image, target image and random noise image, respectively;  $(x, y, k)$  denotes the pixel location  $(x, y)$  of the  $k$ -th frame image.

In addition, when the detection distance is far enough, the target on infrared sensor presents a small spotlike blob occupying only a few pixels. For instance, if the distance of an aircraft or missile is over 8 km, whether it is detected by medium-wave infrared sensor or long-wave infrared sensor, the target is a dim small point. Furthermore, due to the atmosphere refraction, dispersion and absorption, the distribution of target pixels is closer to Gaussian distribution. To simplify the modeling, the widely used two-dimensional Gaussian intensity model is used to describe infrared small target, and it is defined as follows:

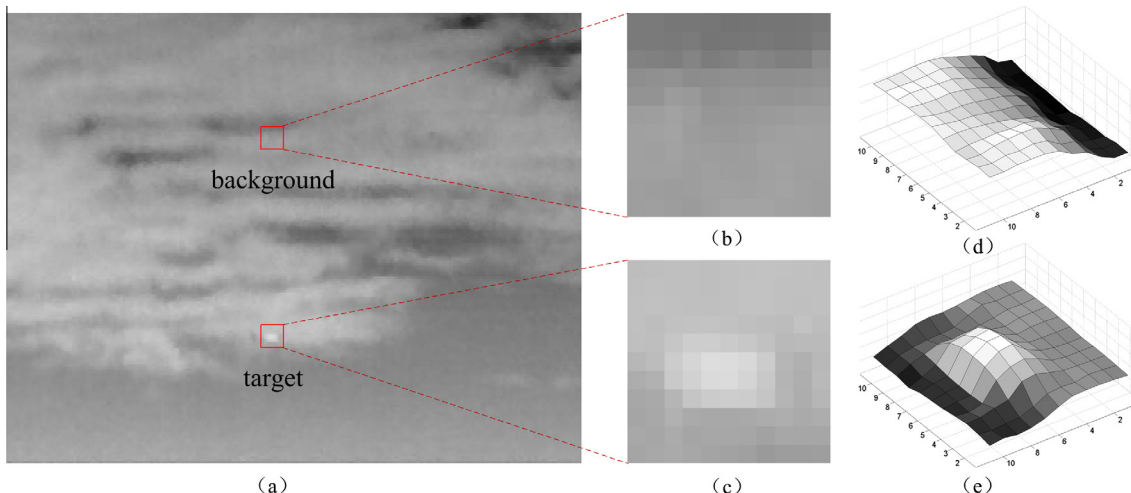


**Fig. 1.** Infrared small target image exhibition (a) one frame infrared image, (b) local region of background, (c) local region of target, (d) 3-D mesh surfaces of (b) and (e) 3-D mesh surfaces of (c).

$$g(x, y) = g_{\max} \exp \left( -\frac{1}{2} \left[ \frac{(x - x_0)^2}{\sigma_x^2} + \frac{(y - y_0)^2}{\sigma_y^2} \right] \right) \quad (2)$$

where  $(x_0, y_0)$  is the target center position;  $g_{\max}$ ,  $\sigma_x$ ,  $\sigma_y$  are the peak intensity, horizontal and vertical standard deviation, respectively.

### 3.2. Target-background separation via RPCA

As a popular feature extraction tool, principal component analysis (PCA) is widely used in various fields, such as pattern recognition, image processing, machine learning, and fault diagnosis. However, PCA can offer the best low-rank representation of the given data matrix in low-dimensional linear subspace when the data is only corrupted by small Gaussian noise. If a given data matrix is under large corruption, PCA method will break down [39]. Consequently, robust principal component analysis (RPCA) has attracted great attention of researchers to recover a low-rank matrix  $L$  from corrupted observations  $D = L + S$ , where some entries of  $S$  might be arbitrarily large magnitude, but are assumed to be sparse [40].

As a result, the single objective optimization problem of PCA turns into a bi-objective optimization problem of RPCA:

$$\min_{LS} (\text{rank}(L), \|S\|_0) \quad \text{s.t.} \quad D = L + S \quad (3)$$

where  $\text{rank}(\cdot)$  is a function for computing rank number of given data matrix, and  $\|\cdot\|_0$  represents the  $\ell^0$ -norm, which can be formulated by equation  $\|S\|_0 = \#\{i, j : a_{ij} \neq 0\}$ . In order to reduce the complexity degree, a weighting parameter  $\lambda$  is introduced, and the bi-objective optimization problem could be converted to a single objective optimization problem [40]:

$$\min_{LS} \text{rank}(L) + \lambda \|S\|_0 \quad \text{s.t.} \quad D = L + S \quad (4)$$

Furthermore, the nuclear norm is the convex envelope of the rank function [41], and  $\ell^1$ -norm is the convex envelope of the  $\ell^0$ -norm on the unit ball. Thus, RPCA seeks sparse and low-rank matrix decomposition by solving:

$$\min_{LS} \|L\|_* + \lambda \|S\|_1 \quad \text{s.t.} \quad D = L + S \quad (5)$$

where  $\|\cdot\|_*$  denotes the nuclear norm, and it is calculated by equation  $\|L\|_* = \sum_k \sigma_k(L)$ ;  $\|\cdot\|_1$  represents the  $\ell^1$ -norm, and it is calculated by equation  $\|S\|_1 = \max_j \sum_i |a_{ij}|$ .

Nowadays, RPCA has been widely used in background modeling, shadows removing, image alignment, etc. In all these applications, more than one entire image are vectored and regarded as observation columns to form a matrix. Since there are high linear correlations of these images, the low rank of the matrix is expected. We focus on infrared small target detection based on single-frame image; however, the conventional RPCA application method is not applicable in this study. Based on previously discussion, the background, targets and noise of infrared small target images could be regarded as low-rank matrix, sparse matrices, respectively. Each column of infrared small target image is taken as an observation due to the strong correlation between them, thus the infrared small targets and noise which corrupt only a few observations will be detected by utilizing the correlation of columns. With these considerations in mind, the infrared small target image model (1) can be converted to a simplified mathematical formulation:

$$D = L_b + S_t + S_n \quad (6)$$

where  $L_b$ ,  $S_t$ ,  $S_n$  represent the low-rank background image matrix, sparse target image matrix and sparse noise image matrix, respectively. As a matter of fact, all entries of  $L_b$  and  $S_t$  should be restricted to non-negative values, while  $S_n$  does not have this restriction.

In general, the low-rank background matrix could be considered as baseline image, while target and noise matrices would be treated as effects on the background matrix. Further, the effects could be divided into positive effect (+) and negative effect (-). As a result, the target and noise matrix can be decomposed into two parts, respectively:

$$S_t = S_t^+ + S_t^-, \quad S_n = S_n^+ + S_n^- \quad (7)$$

Moreover, the positive effect of target could be combined with the positive effect of noise, and the negative effect of target could be combined with the negative effect of noise:

$$S_+ = S_t^+ + S_n^+, \quad S_- = S_t^- + S_n^- \quad (8)$$

Consequently, the simplified mathematical formulation given above (6) is turn into a new one called target-background separation (T-BS) model, as shown in Fig. 2:

$$D = L_b + S_+ + S_- \quad (9)$$

In this study, we focus attention on the positive effect matrix  $S_+$  extraction of target and noise by recovering the observation matrix  $D$  which is the sum of low-rank component  $L_b$  and sparse component ( $S_+ + S_-$ ), thus the convex optimization Eq. (5) will be modified as follows:

$$\min_{L_b, (S_+ + S_-)} \|L_b\|_* + \lambda \|S_+ + S_-\|_1 \quad \text{s.t.} \quad D = L_b + S_+ + S_- \quad (10)$$

and then expressed in the following form:

$$\min_{L_b, (S_+ + S_-)} \|L_b\|_* + \lambda \|S_+ + S_-\|_1 \quad \text{s.t.} \quad \|D - (L_b + S_+ + S_-)\|_2^2 < \varepsilon \quad (11)$$

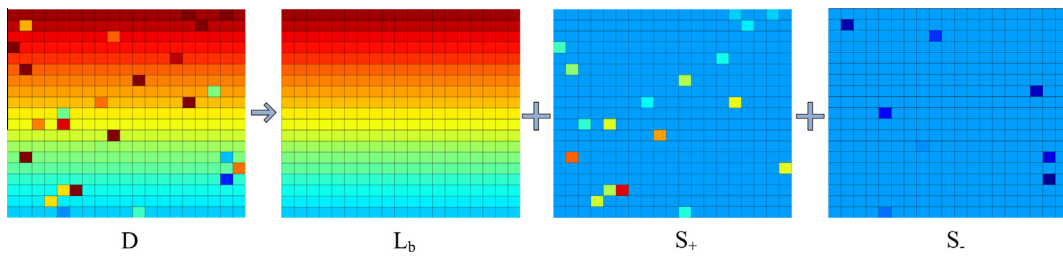


Fig. 2. Target-background separation diagram.

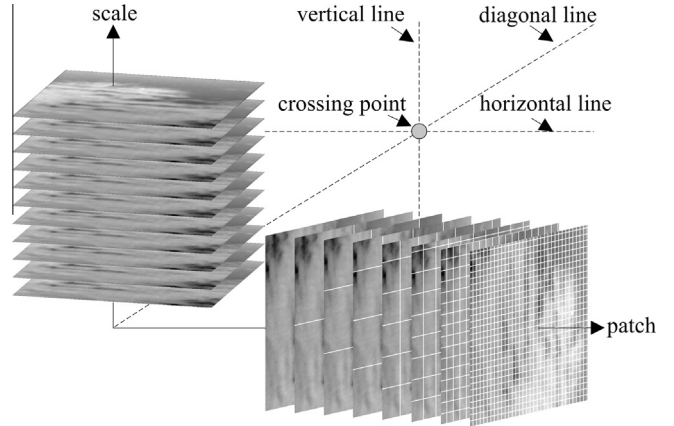


Fig. 3. Pool of image patches for infrared small target detection.

### 3.3. Solution of the T-BS

As mentioned earlier, the constrained optimization problem (11) over infrared small target image is the key to achieve target-background separation, but it is difficult to solve directly. Angshul in [42] provided an iterative solution of the constrained optimization problem by iteratively solving a series of unconstrained versions, which can be converted into:

$$\min_{L_b, (S_+ + S_-)} \|y - (L_b + S_+ + S_-)\|_2^2 + \lambda(\|L_b\|_* + \gamma\|S_+ + S_-\|_1) \quad (12)$$

As a famous iterative solution, Landweber iteration can be used to solve the unconstrained problem. Due to the negative effect of sparse component  $S_-$  is set to zero in each iteration, the unconstrained optimization problem can be expressed in the following form:

$$\min_{L_b, S_+} \|\hat{L}_b + \hat{S}_+ - L_b - S_+\|_2^2 + \frac{\lambda}{\alpha}(\|L_b\|_* + \gamma\|S_+\|_1) \quad (13)$$

And then, the problem can be decomposed into two problems:

$$L_b^{k+1} = \min_{L_b} \|\hat{L}_b + \hat{S}_+ - L_b - S_+^k\|_2^2 + \frac{\lambda}{\alpha}\|L_b\|_* \quad (14)$$

$$S_+^{k+1} = \min_{S_+} \|\hat{L}_b + \hat{S}_+ - L_b^{k+1} - S_+\|_2^2 + \frac{\lambda\gamma}{\alpha}\|S_+\|_1 \quad (15)$$

where  $S$  is the sparse component result of the  $k$ -th iteration prior to set negative numbers to zero.

In order to solve the convex optimization problem of target-background separation, two loops are used to devise a target-background separation algorithm. The inner loop is used for minimizing the unconstrained problem, and the outer loop adopts a cooling technique to solve the constrained problem, as shown in Algorithm 1.

**Algorithm 1.** Solution of Target-Background Separation

---

**Input:** vectorized image  $y$ , weighting parameter  $\lambda$   
**Output:** separated sparse target and low-rank background images

- 1: Initialize: low-rank component  $L_b$ , sparse component  $S_+$ , regularization parameter  $r$ , cooling parameter  $c$ , tolerance error  $\varepsilon$ , tolerance level  $t$ , cooling decrease factor  $d$
- 2: Define objective function:  

$$J = \|y - (\text{vector}(L_b + S_+))\|_2^2 + c \times (\|L_b\|_* + \lambda \times \|\text{vector}(S_+)\|_1)$$
, and calculate  $J_0$
- 3: **While**  $\|y - (\text{vector}(L_b + S_+))\|_2^2 > \varepsilon$
- 4:   **Do**
- 5:     Perform Landweber iteration:  

$$\hat{L}_b + \hat{S}_+ = L_b^k + S_+^k + 1/r \times (y - (L_b^k + S_+^k))$$
- 6:     Singular value thresholding:  

$$\sum = \text{diag}(\text{sign}(\text{diag}(\Lambda)) \cdot \max(0, |\text{diag}(\Lambda)| - c/2r))$$
 where  

$$\hat{L}_b + \hat{S}_+ - S_+^k = U \Lambda V^T$$
- 7:     Update low rank component:  $L_b^{k+1} = U \begin{bmatrix} \sum & 0 \\ 0 & 0 \end{bmatrix} V^T$
- 8:     Update sparse component:  

$$S_+^{k+1} = \text{matrix}(V_s - V_s ./ (2r/\lambda c \times |V_s| + 1))$$
 where  

$$V_s = \text{vector}(\hat{L}_b + \hat{S}_+ - L_b^{k+1})$$
- 9:     Set negative numbers to zero:  

$$S_+^{k+1} = S_+^{k+1} (s = 0 \mid s \in S_+^{k+1} \text{ and } s < 0)$$
- 10:   Calculate objective function value:  $J_{k+1}$
- 11:   **End While**  $(J_k - J_{k+1})/(J_k + J_{k+1}) > t$
- 12:   Decrease cooling parameter:  $c = d \times c$
- 13: **End While**

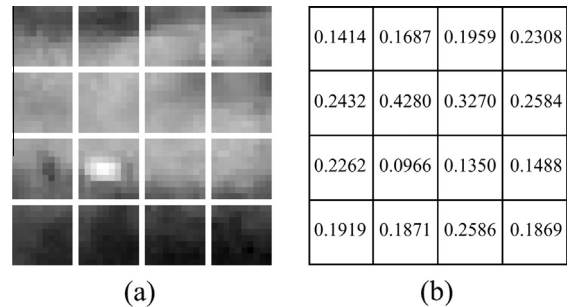
---

**4. Adaptive detection method of infrared small targets****4.1. Image patch set for small target detection**

In this section, multi-scale transform and patch transform are used to generate an image patch set for infrared small target detection.

Although infrared small target is presented as spotlike feature, there is no way to know its priori size on image; furthermore, its size would be variable more or less in the image sequence for continuous observation of the same target. As for small target detection of human participation, the above problem could be addressed with the help of multi-resolution property of human visual system (HVS). If one aims to develop automatic detection method of infrared small target, multi-scale image representation could provide a basic tool for adaptive analyzing target information at one appropriate or several interesting scales [43].

Considering from another side, one whole image of infrared small target can be broken into overlapping or non-overlapping patches by the patch transform [44], and the subsequent image processing procedure for infrared small target detection will be applied in the patch domain, so the different scale images which come from above discussed multi-scale space will be manipulated. By utilizing the sliding window, overlapping image patches can be sampled from the whole image. The size of each image patch is as the same as the size of sliding window. The total number of image patches depends on the size of whole image, size of sliding window and sliding steps in the horizontal and vertical direction. In some special cases, the width or height of whole image is not an integral multiple of the steps in horizontal or vertical direction, respectively, thus there will use the constrained steps with rest width or height.

**Fig. 4.** Image complexity evaluation diagram.

Based on the aforementioned discussion, the scale axis of multi-scale transform and the patch axis of patch transform can be integrated into a chart to form a pool of image patches for small target detection, as shown in Fig. 3. In the chart, the value of scale axis represents the scale parameter value of two-dimensional Gaussian function for the multi-scale transform, and the value of patch axis represents the total number of image patches for the patch transform over one whole image. Obviously, the scale axis and the patch axis both can only take discrete values.

Notice that the entity in the pool of image patches is not a single patch but overlapping or non-overlapping image patches transformed by one whole image with a certain scale. The entity could be regarded as a crossing point of a horizontal line with a certain scale value, and a vertical line with a certain patch value, as illustrated in Fig. 3. That is, each crossing point denotes an image patch set with a certain scale value and a certain patch value. From this analogy, the horizontal line denotes the image patch set with a certain scale value and all the patch value; the vertical line denotes the image patch set with all the scale value and a certain patch value; the diagonal line denotes the image patch set with all the scale value and patch value. In this study, a vertical line for infrared small target detection will be chosen. In the image patch set, the patches are generated by multi-scale transform and patch transform with a certain patch value for each scale image. In some special cases, the infrared small target detection will process over single scale and/or whole image when their values reduce to 1.

Compared to the target-background separation over whole image, there are four important benefits to perform the processing over image patches:

- (1) The target-background separation at the patch level can better take advantages of the local information of image. The dimension of columns regard as the observation is reduced. It leads the low-rank property of the background matrix to be more obvious.
- (2) The size of image matrix for target-background separation via RPCA is confined by the size of the sliding window, thus the computational complexity is reduced, as well as running time of each patch.
- (3) The weighting parameter of RPCA no longer adopts the global uniform value, but chooses appropriate value according to the complexity of each patch.
- (4) The image processing at the patch level is more suitable for parallel computing in the multi-core systems to increase the speed of target-background separation even in real time.

**4.2. Adaptive regulation of weighting parameter**

The target-background separation over each patch is the key procedure for infrared small target detection. However, either the low-rank property of background image or the sparse degree of target image is not consistent in each patch. To choose an

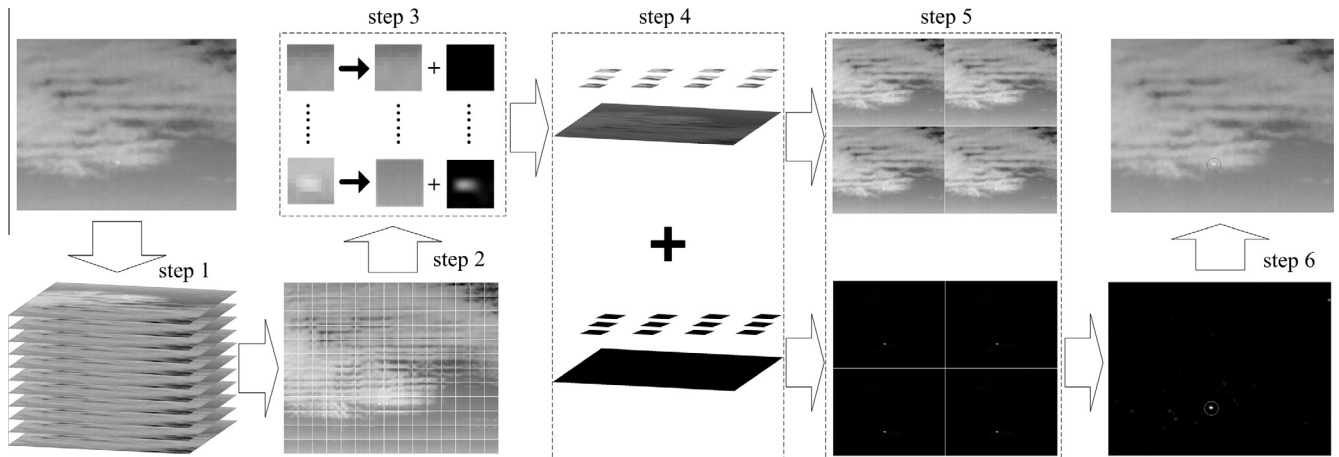


**Fig. 5.** The overview of the proposed infrared small target detection method.

appropriate local weighting parameter for different patches is wiser than to adopt global uniform value, which will better trade-off the low-rank component and the sparse component. After analyzing Eq. (11), a positive correlation exists between the low-rank component and weighting parameter, while the relationship between the sparse component and weighting parameter is negative correlation. However, the weighting parameter is set to  $1/\sqrt{m}$  (where  $m$  is the row number of image) in conventional RPCA application [35], while it does not have the ability to adjust the value of weighting parameter according to the probability whether an image patch contains targets or not. Based on this consideration, the image complexity with different scales and the size of image patches are introduced to evaluate the low-rank property and the sparse degree. The image complexity is integrated with the saliency level of target in the background for adaptive regulation of weighting parameter.

The image entropy is a statistical measure of image gray-value randomness, and the more uniform gray-value probability distribution means the greater image entropy. Nowadays, the image entropy has been adopted to illustrate the complexity of infrared small target image, and the higher value of image entropy indicates the more complex infrared small target image [37,45]. The image entropy is defined as:

$$H = -\sum_{s=0}^{255} p_s \log p_s, \quad \text{when } p_s = 0, \text{ define } p_s \log p_s = 0 \quad (16)$$

where  $p_s$  is the probability of the gray level  $s$  in the whole image. For multi-scale images, research results show that the value of scale parameter represents the value of image entropy.

However, the entropy over whole image is not fit for complexity evaluation of infrared small target image in which each column of image matrix is regard as an observation. Taking this fact into account, the standard deviation of column entropy is used to evaluate the image complexity. Here, the column entropy  $H_j$  denotes the entropy of the  $j$ -th column in an image. Subsequently, the image complexity evaluation can be achieved by calculating the standard deviation of column entropy, and it is expressed as:

$$C = \sqrt{\frac{1}{W} \sum_{j=1}^W (H_j - \mu)^2} \quad (17)$$

where  $w$  is the width of image, and  $\mu$  is the mean of all column entropy. In order to intuitively show the effectiveness of the image complexity evaluation, and a diagram is given in Fig. 4.

Additionally, the size of image patches cannot be ignored for the weighting parameter regulation, because it has effects on the

sparse degree of small target in the image. In general, the size of image patches can be measured by standard small target size, and the Society of Photo-Optical Instrumentation Engineers (SPIE) defines the small target as having a total spatial extent of less than 80 pixels [46,47]. Consequently, the size of image patches turns into:

$$T = \frac{\phi}{80} \times (w \times h) \quad (18)$$

where  $\phi$  is the reference pixels number of target  $\phi = 40$  in general, while if the target is not a small target obviously, the value should be adjusted to appropriate size;  $w, h$  are the width and height of image patch, respectively.

Based on the above discussion, the weighting parameter for target-background separation over each patch would be regulated adaptively, and the value can be calculated from the following formula:

$$\lambda = \psi \times \left( \frac{C}{H} \right)^\alpha \times T^\beta \quad (19)$$

where  $\psi$  represents the saliency level of target in the background, and it recommends an value in range of  $1 \leq \psi \leq 5$ , and the smaller value, the more saliency;  $\alpha, \beta$  are constant. In this study,  $\alpha = 0.45$  and  $\beta = -0.12$  are empirical values. In the further research, some new evaluation standards and more accurate parameter values would be adopted.

#### 4.3. Comprehensive scheme and implementation

Based on the aforementioned preparation, target-background separation can be achieved over image patch set by using adaptive weighting parameter, and then infrared small target detection is realized by threshold segmentation of template matching similarity measurement over the entire separated target image. The overview of infrared small target detection method proposed in this paper is depicted in Fig. 5, and the steps are expounded as follows:

In the first step, the original single-frame infrared small target image will be processed by multi-scale transform to construct multi-scale space for handling the unknown and/or variable size of infrared small target.

In the second step, the different scale images from multi-scale space will be broken into overlapping patches by patch transform. Accordingly, a pool of image patches for small target detection is formed after previous two steps.

In the third step, the target-background separation is carried out over an image patch set from the above generated pool using adaptive weighting parameter.

In the fourth step, the separated target and background patches from the same scale image will be reconstructed to entire separated background and target images with certain scale, respectively.

In the fifth step, image fusion algorithm will be employed to fuse two or more entire separated images of different scales, thus the separated target and background images will be obtained. In this study, different fusion strategies are adopted for low-rank background image and sparse target image. Two-dimensional wavelet transform is used to decompose the separated background images of different scales to get the low and high frequency subband coefficients, and then these coefficients are computed by weighted average for low frequency and maximum absolute value for high frequency. The weighted average of fused subband coefficients is defined as:

$$w_i = \begin{cases} w_a & i = 1 \\ ((i^\gamma - 1) \times w_{i-1} + w_b) / i^\gamma & i > 1 \end{cases} \quad (20)$$

where  $w_a$ ,  $w_b$  are the subband coefficients of the first image and a new addition image, respectively;  $\gamma$  is a constant,  $\gamma = 2$  is chosen in this study. The maximum absolute value of fused subband coefficients is iteratively computed by:

$$w_i = \begin{cases} w_a & i = 1 \\ w \cdot \max\{|w_{i-1}|, |w_b|\} & i > 1 \end{cases} \quad (21)$$

At the same time, the separated target images of different scales are selected under the rules of maximum kurtosis in view of the fact that kurtosis describes the flatness of the gray level compared with the standard distribution, and the kurtosis can be written as:

$$K = \frac{1}{w \times h} \sum_{x=1}^w \sum_{y=1}^h \left( \frac{I(x, y) - \mu_I}{\sigma_I} \right)^4 \quad (22)$$

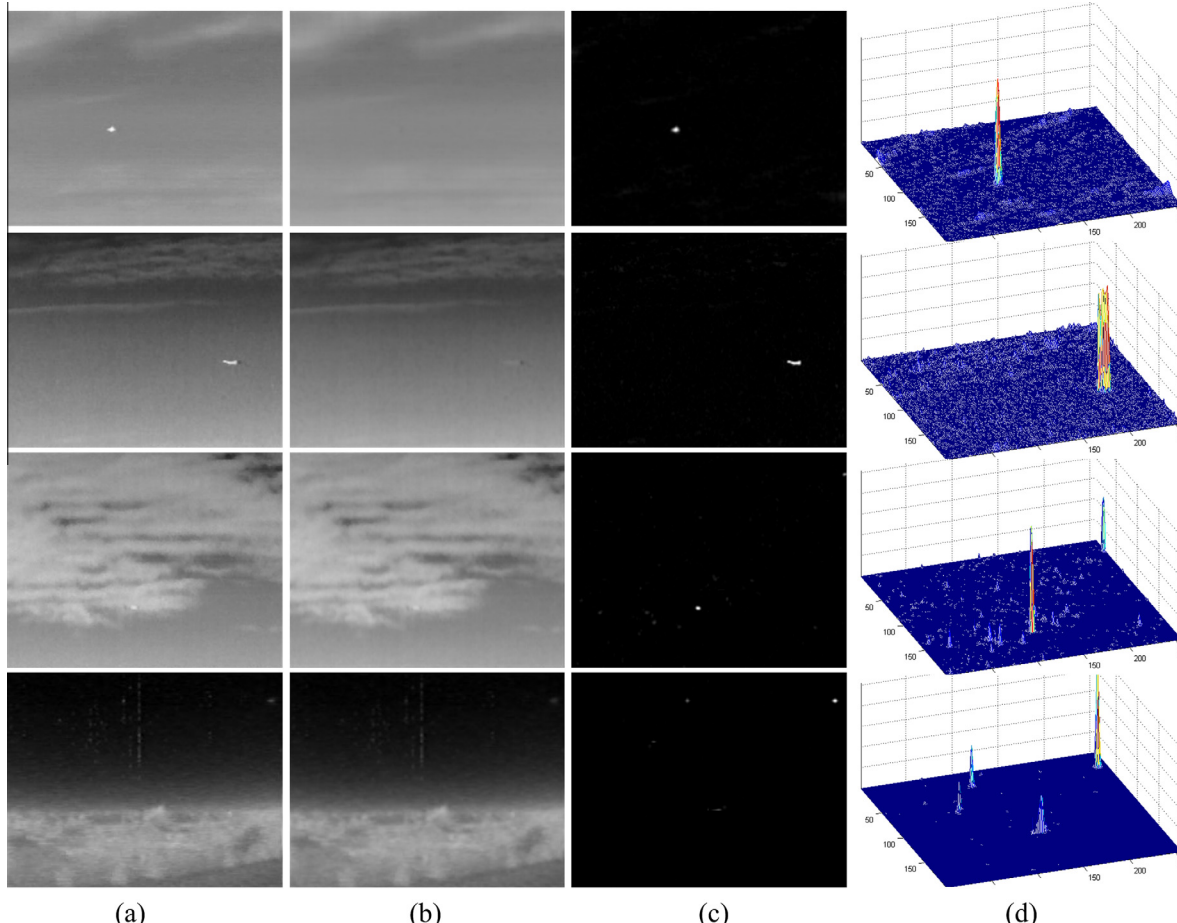
where  $w$ ,  $h$  are the width and height of entire image;  $I(x, y)$  denotes the intensity of pixel  $(x, y)$ , as well as  $\mu_I$ ,  $\sigma_I$  represent the average and standard deviation of entire image intensity, respectively.

In the final step, the infrared small target detection is achieved by threshold segmentation of template matching similarity measurement over the entire separated target image. The aforementioned 2-D Gaussian model is regarded as the matching template, and the cosine similarity measurement  $\xi$  is used to evaluate the similarity between suspected target region and template image [48]. The cosine similarity can be calculated from the following formula:

$$\xi = \frac{\sum_{x=1}^w \sum_{y=1}^h R(x, y) \times g(x, y)}{\sqrt{\sum_{x=1}^w \sum_{y=1}^h R(x, y)^2} \sqrt{\sum_{x=1}^w \sum_{y=1}^h g(x, y)^2}} \quad (23)$$

where  $R(x, y)$  is the suspected target region, and  $w$ ,  $h$  are the width and height of template image, respectively.

To be sure, if the background image is useless, the corresponding image reconstruction and fuse procedures should be omitted to reduce the computation.

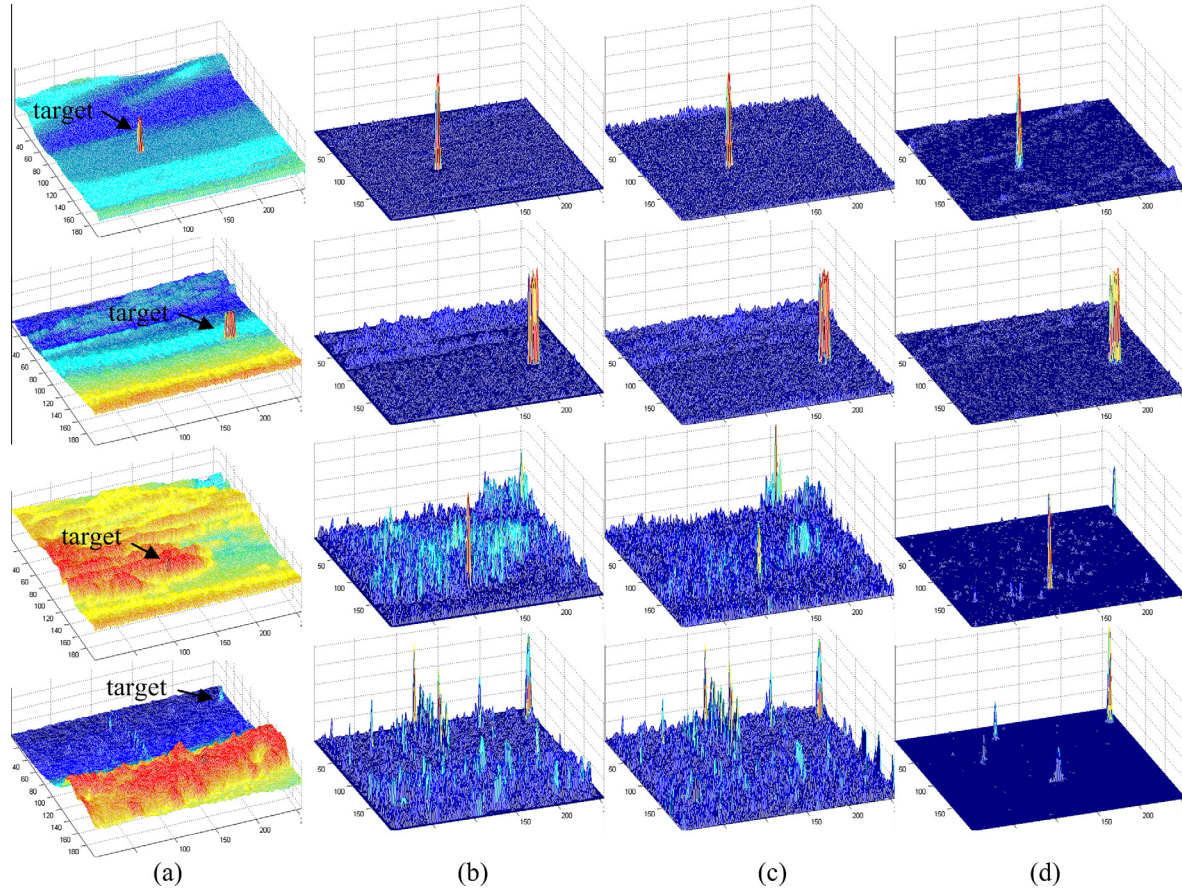


**Fig. 6.** Target-background separation experiment results (a) original image, (b) low-rank background, (c) sparse target and (d) 3-D mesh surfaces.

**Table 1**

Time cost of target-background separation (in seconds).

| Scale number | Patch size | Sliding steps | The 1st image  |            | The 2nd image  |            | The 3rd image  |            | The 4th image  |            |
|--------------|------------|---------------|----------------|------------|----------------|------------|----------------|------------|----------------|------------|
|              |            |               | Time per patch | Total time |
| 1            | 200 * 256  | 200, 256      | 3.8327         | 3.8327     | 3.9634         | 3.9634     | 3.5522         | 3.5522     | 4.2644         | 4.2644     |
| 1            | 128 * 128  | 128, 128      | 1.2270         | 4.9079     | 1.2050         | 4.8200     | 1.0923         | 4.3690     | 1.3114         | 5.2457     |
| 3            | 128 * 128  | 64, 64        | 1.1705         | 31.6034    | 1.1595         | 31.3069    | 1.0511         | 28.3793    | 1.2363         | 33.3813    |
| 3            | 64 * 64    | 64, 64        | 0.2777         | 13.3279    | 0.2843         | 13.6453    | 0.2700         | 12.9595    | 0.3023         | 14.5093    |
| 6            | 64 * 64    | 32, 32        | 0.2695         | 67.9210    | 0.2823         | 71.1462    | 0.2608         | 65.7182    | 0.3118         | 78.5825    |
| 6            | 32 * 32    | 32, 32        | 0.0830         | 27.8752    | 0.0873         | 29.3448    | 0.0813         | 27.3161    | 0.1000         | 33.6053    |

**Fig. 7.** 3-D mesh surfaces results of background clutter suppression experiment (a) original image with no-noise, (b) LMR, (c) Top-hat and (d) our proposed method.**Table 2**

Performance evaluation of background clutter suppression.

| Metrics            | The 1st image |         |              | The 2nd image |         |              | The 3rd image |         |              | The 4th image |         |              |
|--------------------|---------------|---------|--------------|---------------|---------|--------------|---------------|---------|--------------|---------------|---------|--------------|
|                    | LMR           | Top-hat | Our method   |
| SCR <sub>in</sub>  | 1.56          | 1.56    | 1.56         | 1.15          | 1.15    | 1.15         | 1.92          | 1.92    | 1.92         | 0.68          | 0.68    | 0.68         |
| SCR <sub>out</sub> | 8.81          | 10.13   | <b>14.20</b> | 7.60          | 9.09    | <b>13.03</b> | 3.10          | 2.80    | <b>14.04</b> | 3.43          | 3.12    | <b>15.04</b> |
| ISCR               | 5.65          | 6.49    | <b>9.10</b>  | 6.64          | 7.94    | <b>11.37</b> | 1.62          | 1.46    | <b>7.32</b>  | 5.06          | 4.60    | <b>22.19</b> |
| BSF                | 3.26          | 2.97    | <b>3.37</b>  | 4.79          | 4.89    | <b>6.38</b>  | 1.12          | 1.61    | <b>6.03</b>  | 4.43          | 4.36    | <b>19.51</b> |

Bold fonts indicate the best performance.

## 5. Experimental results and analysis

### 5.1. Experiment scheme and evaluation metrics

In this section, three kinds of experiments are performed to evaluate the performance of the proposed infrared small target detection method. Several infrared small target images with different background and some groups of sequence are tested. The first

experiment is performed to validate the target-background separation performance of the proposed method. The second experiment is carried out to illustrate the background clutter suppression performance by three types of metrics with no-noise and added-noise conditions. The performance of the proposed method is compared with two classical methods. The third experiment is performed to demonstrate the detection performance. The detection probability and false alarm rate are used for evaluation, and three methods are

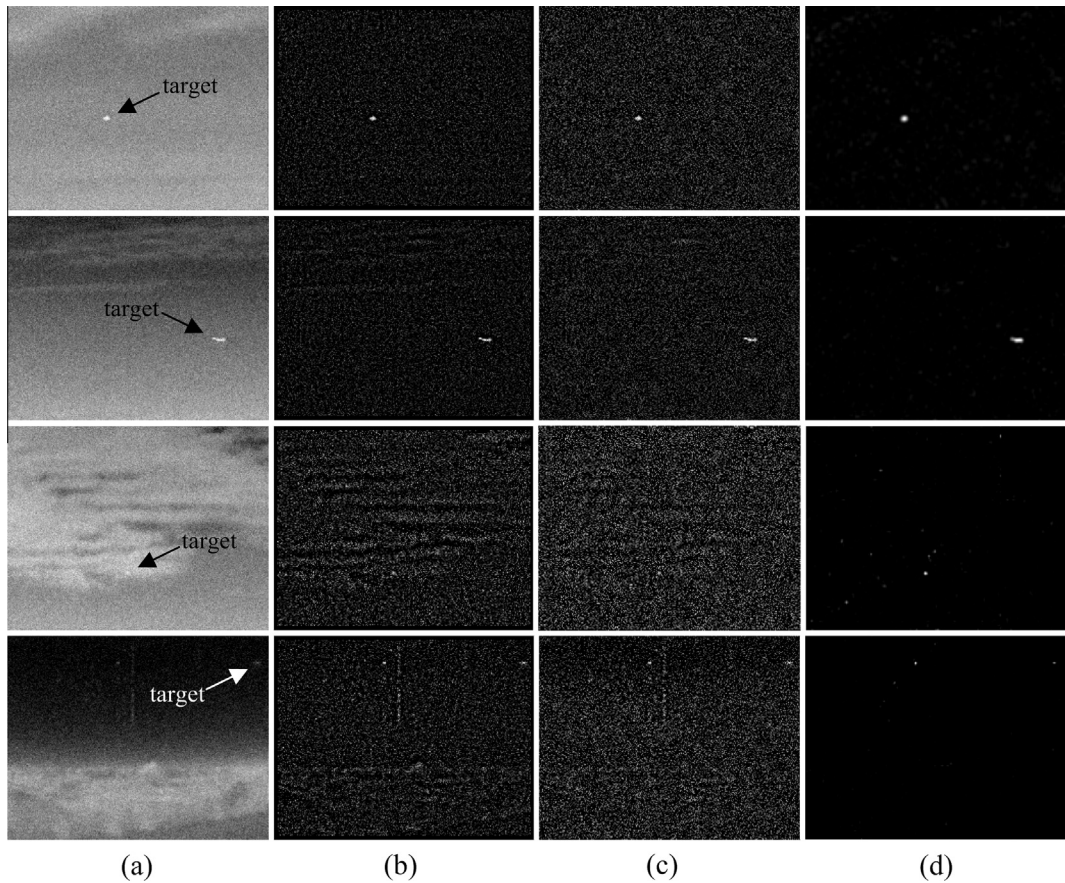


**Fig. 8.** Background clutter suppression experiment results (a) original image with added-noise, (b) LMR, (c) Top-hat and (d) our proposed method.

taken as baseline methods. All the experiments were conducted on a PC with 4-GB memory and 3.0-GHz Intel Core2 Duo processor E8400, and the code was implemented by MATLAB R2012a software.

A good infrared small target detection method can clearly suppress background clutter and enhance target intensity. In order to validate the background clutter suppression performance of proposed method, three types of metrics: signal-to-clutter ratio (SCR), improvement of signal-to-clutter ratio (ISCR), background suppression factor (BSF) are adopted [49]. The SCR represents the difficulty of infrared small target detection, and it is defined by:

$$\text{SCR} = \frac{|\mu_t - \mu_I|}{\sigma_I} \quad (24)$$

where  $\mu_t$  is the average of target region intensity;  $\mu_I, \sigma_I$  are the average and standard deviation of whole image intensity, respectively. Subsequently, the ISCR can be used to measure the improvement of SCR before ( $\text{SCR}_{in}$ ) and after ( $\text{SCR}_{out}$ ) processing, it is defined as follows:

$$\text{ISCR} = \frac{\text{SCR}_{out}}{\text{SCR}_{in}} \quad (25)$$

Furthermore, the BSF estimates the amount of background clutter suppression, it is expressed as:

$$\text{BSF} = \frac{\sigma_{in}}{\sigma_{out}} \quad (26)$$

where  $\sigma_{in}, \sigma_{out}$  denote the standard deviation of whole image intensity before and after processing, respectively.

In order to further evaluate the detection performance of the proposed method, two most important metrics: detection

probability  $P_d$  and false alarm rate  $F_a$  are introduced, and they are defined as following:

$$P_d = \frac{\text{number of true detections}}{\text{number of actual targets}} \quad (27)$$

$$F_a = \frac{\text{number of false detections}}{\text{number of frame insequence}} \quad (28)$$

## 5.2. Performance evaluation and comparative analysis

### 5.2.1. Target-background separation experiment

Four types of infrared small target images with different cloudy sky background, which are denoted by 1st, 2nd, 3rd and 4th image from top to bottom, are tested to validate the effectiveness of the proposed target-background separation method. The size of images are all  $200 \times 256$ . In multi-scale transform procedure, the scale number, filter size, minimum standard deviation and standard deviation step are 6, 7, 0, and 0.4, respectively; In patch transform procedure, the size of sliding window is  $64 \times 64$ , and the steps in vertical and horizontal direction are all 32; In target-background separation procedure,  $r = 1, c = \max |y|, \varepsilon = 1e-6, t = 1e-4$  and  $d = 0.5$  are chosen in this study, and the saliency level for adaptive regulation of weighting parameter over the above four images are 1, 2, 3 and 5, respectively.

Experiment results are reported as shown in Fig. 6. In this figure, column (a) shows the four original images with different background. From top to bottom, the background becomes more complex, in other words, it is more difficult to detect the target. Subsequently, column (b) and (c) are the separated low-rank

background and sparse target, respectively. It can be clearly seen that the proposed target-background separation method could obtain good separation results. In order to intuitively show the separated target images, the column (d) presents three-dimensional (3-D) mesh surfaces of the corresponding images in column (c).

In order to analyze the time cost of target-background separation, the average time consumption of image patches are counted statistically over four images with different scale numbers, patch sizes and sliding steps, as shown in Table 1. It is observed that there are more and more total time cost as the larger scale number, smaller patch size and sliding steps, especially, it is more notable for the smaller patch size. Nevertheless, the average time cost per image patch is reduced, and predictably, it will lead to less time cost under the environment of parallel computing, in which the image patches can be processed simultaneously. Additionally, the space cost in the procedure of target-background separation is also related with the scale number, patch size and sliding steps. It is less than three times the product of scale number, patch number and patch size.

### 5.2.2. Background clutter suppression experiment

The proposed target-background separation method could be regard as a method of background clutter suppression for infrared small target detection. Two well studied baseline methods: LMR [6] and Top-hat [8] are used to compare background clutter suppression performance with the proposed method over four benchmark infrared small target images under the condition of no-noise and added-noise.

Firstly, the background clutter suppression experiment over the above four images with no-noise are performed, and the 3-D mesh surfaces results are shown in Fig. 7. These results show that all three methods can suppress background clutter with similar performance of the 1st and 2nd images, while the proposed method can clearly suppress background clutter than two baseline methods for the 3rd and 4th images. In spite of the background is more complex one by one from top to bottom, as well as the target is less saliency, the background clutter suppression performance of the proposed method is more stable than two baseline methods.

For quantitative evaluation and comparison, the aforementioned metrics SCR, ISCR, BSF are adopted to measure the performance of the three methods. Table 2 shows the experiment results of the four types of infrared small target images with different background. These results indicate that the proposed method outperforms the baseline methods in all metrics, especially for the 3rd and 4th image. These results could demonstrate the effectiveness of the proposed method as a background clutter suppression method.

Subsequently, the background clutter suppression experiment over the above four images with added-noise are performed. In this experiment, Gaussian white noise with mean  $\mu = 0$  and variance  $\sigma^2 = 0.3 \times 10^{-3} \sim 6 \times 10^{-3}$  is added to the above four images. Fig. 8 represents the results comparison of three methods under the condition of Gaussian white noise with  $\sigma^2 = 3 \times 10^{-3}$ . We can find that the proposed method has better ability to resist noise than two baseline methods, and it can remove background clutter and noise, but retain the target signal effectively.

We repeated the experiment 50 times with the variance step length 0.0003 of Gaussian white noise. The averages of SCR, ISCR

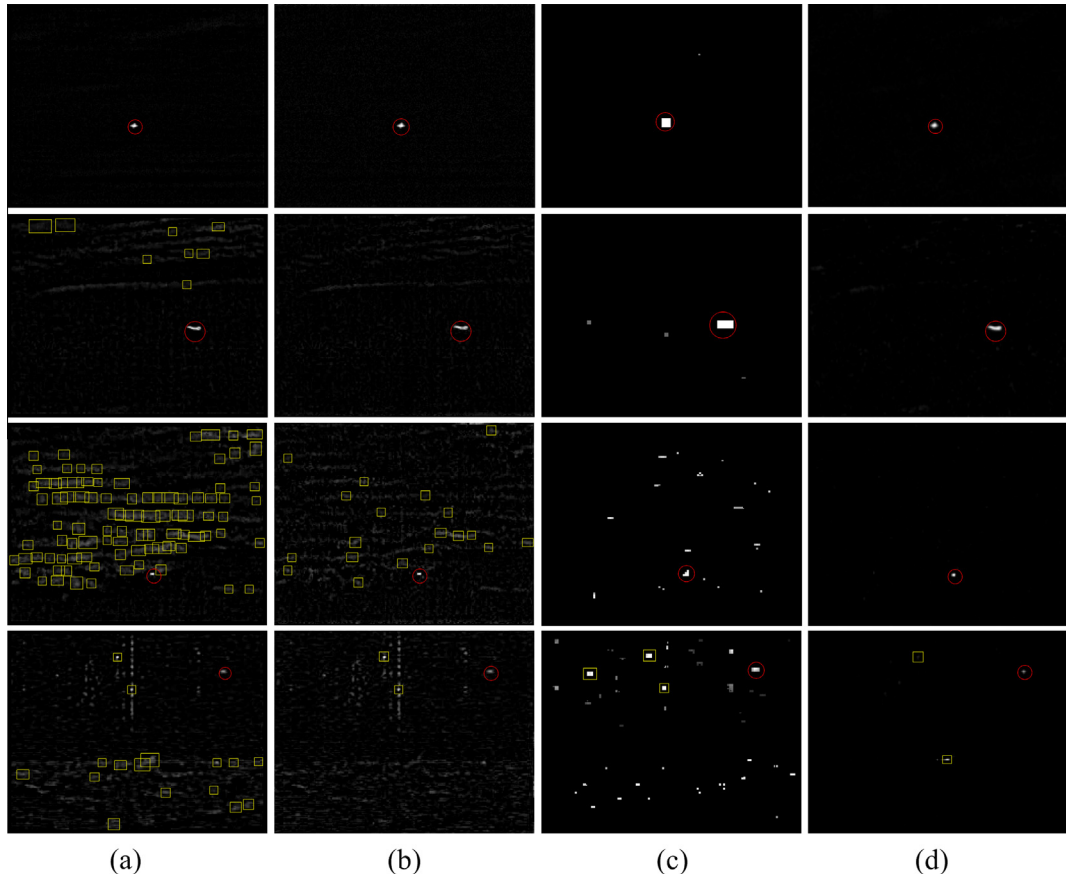


**Fig. 9.** Infrared small target detection experiment results (a) LMR, (b) Top-hat, (c) LCM and (d) our proposed method.

and BSF are counted statistically over four images with added noise. With the incensement of noise level, the SCR of the input images decrease observably, while the performance of proposed method does not reduce correspondingly, and demonstrates its insensitivity to noise, especially for the 1st and 2nd image sequences. In spite of complexity background of the 3rd and 4th image sequences, the performance of proposed method presents fluctuation or depreciation along with the heavier noise level, but is still better than two baseline methods apparently.

### 5.2.3. Infrared small target detection experiment

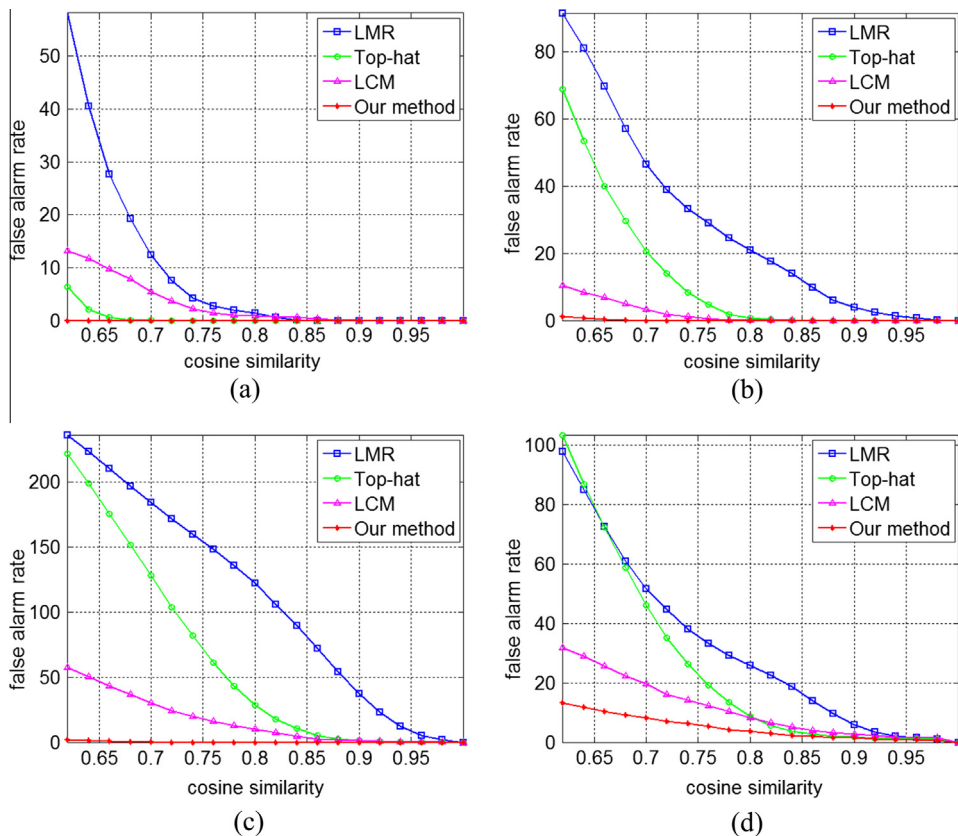
In this experiment, four infrared small target real image sequences, denoted by 1st, 2nd, 3rd and 4th image sequences, are considered to demonstrate the detection performance of the proposed method, and each image sequence contains 30 images with size  $200 \times 256$ . Noticing that the above four images come from these four image sequences as the first frame respectively. As three baseline methods, LMR [6], Top-hat [8] and LCM [3] are used to compare the performance of infrared small target detection. In addition, the infrared imaging sensors are stationary in the 1st and 4th image sequences, while they are mobile in the 2nd and 3rd image sequences. Thus, the background images in the 2nd and 3rd image sequences change more significant than those in the 1st and 4th image sequences.

In the threshold segmentation procedure of temple matching, the cosine similarity range is chosen from 0.6 to 1 with step length 0.02. Due to the target size differences, the effective region searching radius of each suspected target is 5 for the 1st, 3rd and 4th image sequences, while it is 9 for the 2nd image sequence. In order to determine the detected targets are actual targets or not, all

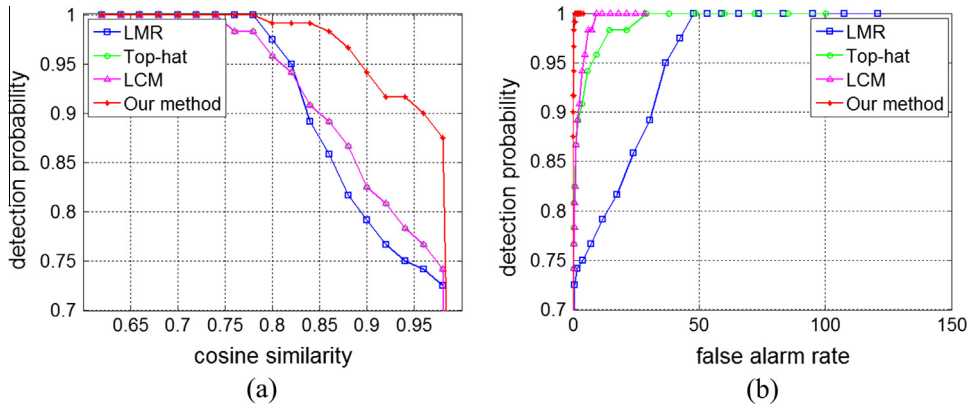
actual targets positions are obtained manually before experiment. When the detected target positions are compared with the actual target positions, a tolerance error with  $(\pm 5, \pm 5)$  pixels around the effective region center is assigned to each target. In order to intuitively show, the detection results of the 10th frame from four image sequences with cosine similarity  $\xi = 0.86$  are given in Fig. 9, in which the true targets and false alarm targets are labeled in red circles and yellow rectangles, respectively.

Fig. 10 shows the curves of false alarm rate  $F_a$  with different cosine similarity  $\xi$  of four detection methods. For all detection methods, the higher cosine similarity leads to lower false alarm rate over four image sequences. It can be observed that the proposed method can generate less false alarm targets than the baseline methods in the same conditions.

On the other hand, the detection probability is also related with the cosine similarity; however, the detection probability of four detection methods all can reach 1 for the 1st, 2nd and 3rd image sequences when the cosine similarity is less than 0.86, while they are 0.43, 0.63, 0.57 and 0.93 for the 4th image sequence with cosine similarity 0.86. Because the gray value of target is not always higher than that of its immediate background in the 4th image sequence, the detection probability of LCM method is reduced. After detection experiments over four image sequences, the average detection probability  $P_d$  under the conditions of different cosine similarity  $\xi$  and different false alarm rate  $F_a$  are calculated, and plotted respectively in Fig. 11. Under the conditions of certain cosine similarity or false alarm rate, the proposed method has higher detection probability than the baseline methods. The detection experiment results illustrate that the proposed method has excellent performance in high



**Fig. 10.** Curves of false alarm rate with different cosine similarity (a) the 1st image sequence, (b) the 2nd image sequence, (c) the 3rd image sequence and (d) the 4th image sequence.



**Fig. 11.** Average detection probability over four image sequences (a) under the condition of different cosine similarity and (b) under the condition of different false alarm rate.

detection probability and low false alarm rate for infrared small target detection.

## 6. Conclusions

In this paper, a new target-background separation model is designed, and then an adaptive detection method of infrared small target is proposed. By multi-scale transform and patch transform, an image patch set can be chosen from the generated pool of image patches. The weighting parameter for target-background separation over each patch is regulated adaptively using the standard deviation of column entropy and the size of image patches. The infrared small target detection problem over entire image is converted into detection over image patches with adaptive weighting parameters. The results of experiments show that the proposed method can suppress the background clutter effectively and achieve stable detection performance. In the future, we will investigate multiprocessor based parallel computing for target-background separation over image patches.

## Conflict of interest

There is no conflict of interest.

## Acknowledgements

This work was partly supported by National Natural Science Foundation of China (Grant Nos. 61273350, U1435220 and 60875072). The authors also gratefully acknowledge the anonymous reviewers for their helpful comments and suggestions which have improved the quality of this manuscript.

## References

- [1] C. Gao, T. Zhang, Q. Li, Small infrared target detection using sparse ring representation, *IEEE Aerospace Electron. Syst. Mag.* 27 (2012) 21–30.
- [2] X.P. Shao, H. Fan, G.X. Lu, J. Xu, An improved infrared dim and small target detection algorithm based on the contrast mechanism of human visual system, *Infrared Phys. Technol.* 55 (2012) 403–408.
- [3] C.P. Chen, H. Li, Y. Wei, T. Xia, Y.Y. Tang, A local contrast method for small infrared target detection, *IEEE Trans. Geosci. Remote Sens.* (2014) 574–581.
- [4] G. Chenqiang, M. Deyu, Y. Yi, W. Yongtao, Z. Xiaofang, A.G. Hauptmann, Infrared patch-image model for small target detection in a single image, *IEEE Trans. Image Process.* 22 (2013) 4996–5009.
- [5] E.J. Candès, X. Li, Y. Ma, J. Wright, Robust principal component analysis?, *J ACM (JACM)* 58 (2011) 1–39.
- [6] J.Y. Chen, I.S. Reed, A detection algorithm for optical targets in clutter, *IEEE Trans. Aerospace Electron. Syst.* (1987) 46–59.
- [7] S.D. Deshpande, H.E. Meng, R. Venkateswarlu, P. Chan, Max-mean and max-median filters for detection of small targets, in: SPIE's International Symposium on Optical Science, Engineering, and Instrumentation, International Society for Optics and Photonics, 1999, pp. 74–83.
- [8] V.T. Tom, T. Peli, M. Leung, J.E. Bondaryk, Morphology-based algorithm for point target detection in infrared backgrounds, in: Optical Engineering and Photonics in Aerospace Sensing, International Society for Optics and Photonics, 1993, pp. 2–11.
- [9] X. Qin, Y. Zhao, K. Yang, H. Wang, Research on IR small target detection and background suppression, in: Information Theory and Information Security (ICITIS), 2010 IEEE International Conference, 2010, pp. 80–83.
- [10] Q. Hanlin, L. Shangqian, Z. Huixin, Background suppression for dim small target with Gabor kernel non-local means, *Infrared Laser Eng.* 38 (2009) 737–741.
- [11] B. Zhang, T. Zhang, Z. Cao, K. Zhang, Fast new small-target detection algorithm based on a modified partial differential equation in infrared clutter, *Opt. Eng.* 46 (2007) 106401 (1–6).
- [12] D.-B. Wang, S.-Q. Liu, X.-M. Kou, M. Hong, Infrared background clutter suppression algorithm of adaptive regularization based on MRF, *J. Infrared Millimeter Waves* 28 (2009) 440–444.
- [13] S. Kim, Analysis of small infrared target features and learning-based false detection removal for infrared search and track, *Pattern Anal. Appl.* (2013) 1–18.
- [14] Y. Cao, R. Liu, J. Yang, Small target detection using two-dimensional least mean square (TDLMS) filter based on neighborhood analysis, *Int. J. Infrared Millimeter Waves* 29 (2008) 188–200.
- [15] T.-W. Bae, Y.-C. Kim, S.-H. Ahn, K.-I. Sohng, An efficient two-dimensional least mean square (TDLMS) based on block statistics for small target detection, *J. Infrared Millimeter Terahz Waves* 30 (2009) 1092–1101.
- [16] Q. Hanlin, Z. Huixin, L. Shangqian, L. Fan, Dim and small target background suppression using bilateral filtering, *High Power Laser Part. Beams* 21 (2009) 25–28.
- [17] W. Zhang, X.-L. Meng, M.-Y. Cong, K.-X. Li, Algorithm of space point target detection for IR scan images, *Infrared Laser Eng.* 38 (2009) 921–925.
- [18] H.-L. Qin, J. Li, H.-X. Zhou, R. Lai, S.-Q. Liu, Infrared dim and small target background suppression using shearlet transform, *J. Infrared Millimeter Waves* 30 (2011) 162–166.
- [19] H.-L. Qin, Y.-H. Liang, H.-X. Zhou, R. Lai, S.-Q. Liu, Infrared small and weak targets background suppression based on surfacelet transform, *Syst. Eng. Electron.* 33 (2011) 2149–2153.
- [20] B. Honggang, Z. Jianqi, W. Xiaorui, Infrared complex background clutter suppression algorithm based on wave atom transform, *High Power Laser Part. Beams* 25 (2013) 37–41.
- [21] A. Ondini, G. Marsiglia, L. Fortunato, G. Balzarotti, Techniques for detection of multiple, extended, and low contrast targets in infrared maritime scenarios, *Opt. Eng.* 45 (2006) 126401 (1–15).
- [22] E. Lee, H.J. Yoo, E. Gu, K.H. Park, Moving dim-target tracking algorithm using template matching, in: 2013 International Conference on Technological Advances in Electrical, Electronics and Computer Engineering (TaeEeCe), 2013, pp. 294–297.
- [23] R. Liu, Y. Lu, C. Gong, Y. Liu, Infrared point target detection with improved template matching, *Infrared Phys. Technol.* 55 (2012) 380–387.
- [24] R. Liu, X. Li, L. Han, J. Meng, Track infrared point targets based on projection coefficient templates and non-linear correlation combined with Kalman prediction, *Infrared Phys. Technol.* 57 (2012) 68–75.
- [25] T. Hu, J.-J. Zhao, Y. Cao, F.-L. Wang, J. Yang, Infrared small target detection based on saliency and principal component analysis, *J. Infrared Millimeter Waves* 29 (2010) 303–306.
- [26] Y. Cao, R.M. Liu, J. Yang, Infrared small target detection using PPCA, *Int. J. Infrared Millimeter Waves* 29 (2008) 385–395.
- [27] Z. Liu, C. Chen, X. Shen, X. Zou, Detection of small objects in image data based on the nonlinear principal component analysis neural network, *Opt. Eng.* 44 (2005) 093604 (1–9).
- [28] C.Q. Gao, H.D. Su, L.X. Li, Q. Li, S. Huang, Small infrared target detection based on Kernel principal component analysis, in: 2012 5th

- International Congress on Image and Signal Processing (Cisp), 2012, pp. 1335–1339.
- [29] S. Kim, Y. Yang, J. Lee, Y. Park, Small target detection utilizing robust methods of the human visual system for IRST, *J Infrared Millimeter Terahz Waves* 30 (2009) 994–1011.
- [30] S. Kim, J. Lee, Scale invariant small target detection by optimizing signal-to-clutter ratio in heterogeneous background for infrared search and track, *Pattern Recognit.* 45 (2012) 393–406.
- [31] X. Wang, L. Xu, Infrared dim target detection based on visual attention, *Infrared Phys. Technol.* 55 (2012) 513–521.
- [32] S.X. Qi, J. Ma, C. Tao, C.C. Yang, J.W. Tian, A robust directional saliency-based method for infrared small-target detection under various complex backgrounds, *IEEE Geosci. Remote Sens.* 10 (2013) 495–499.
- [33] J.H. Han, Y. Ma, B. Zhou, F. Fan, K. Liang, Y. Fang, A robust infrared small target detection algorithm based on human visual system, *IEEE Geosci. Remote Sens.* 11 (2014) 2168–2172.
- [34] X. Dong, X. Huang, Y. Zheng, L. Shen, S. Bai, Infrared dim and small target detecting and tracking method inspired by human visual system, *Infrared Phys. Technol.* 62 (2014) 100–109.
- [35] C.Y. Zheng, H. Li, Small infrared target detection based on low-rank and sparse matrix decomposition, in: P. Yarlagadda, Y.H. Kim (Eds.), *Measurement Technology and Its Application, Pts 1 and 2*, 2013, pp. 214–218.
- [36] C.-Y. Zheng, H. Li, Small infrared target detection based on harmonic and sparse matrix decomposition, *Opt. Eng.* 52 (2013) 066401 (1–11).
- [37] L. Li, H. Li, T. Li, F. Gao, Infrared small target detection in compressive domain, *Electron. Lett.* 50 (2014) 510–512.
- [38] Y. He, M. Li, J. Zhang, Q. An, Small infrared target detection based on low-rank and sparse representation, *Infrared Phys. Technol.* 68 (2015) 98–109.
- [39] Z. Lin, A. Ganesh, J. Wright, L. Wu, M. Chen, Y. Ma, Fast convex optimization algorithms for exact recovery of a corrupted low-rank matrix, *Comput. Adv. Multi-Sensor Adaptive Process. (CAMSAP)* 61 (2009) 1–18.
- [40] J. Wright, A. Ganesh, S. Rao, Y. Peng, Y. Ma, Robust principal component analysis: exact recovery of corrupted low-rank matrices by convex optimization, *Proc. Neural Inf. Process. Syst.* (2009) 1–9.
- [41] M. Fazel, Matrix rank minimization with applications, in: PhD thesis, Stanford University, 2002.
- [42] M. Angshul, A sparsity based approach towards fast MRI acquisition, in: University of British Columbia, 2012.
- [43] T. Lindeberg, Scale-space, *Encyclopedia Comput. Sci. Eng.* IV (2008) 2495–2504.
- [44] C. Taeg Sang, M. Butman, S. Avidan, W.T. Freeman, The patch transform and its applications to image editing, in: *Computer Vision and Pattern Recognition, 2008. CVPR 2008. IEEE Conference on 2008*, 2008, pp. 1–8.
- [45] L. Yang, J. Yang, K. Yang, Adaptive detection for infrared small target under sea-sky complex background, *Electron. Lett.* 40 (2004) 1083–1085.
- [46] Z. Wei, C. Mingyu, W. Liping, Algorithms for optical weak small targets detection and tracking: review, in: *Neural Networks and Signal Processing, 2003. Proceedings of the 2003 International Conference on 2003*, 2003, pp. 643–647.
- [47] H.S. Richardson, Multiple multistage hypothesis tests a sequential detection approach, in: Queen's University, 1992.
- [48] Y.Y. Tang, T. Xia, Y. Wei, H. Li, L. Li, Hierarchical kernel-based rotation and scale invariant similarity, *Pattern Recognit.* 47 (2014) 1674–1688.
- [49] S. Kim, Double layered-background removal filter for detecting small infrared targets in heterogenous backgrounds, *J Infrared Millimeter Terahz Waves* 32 (2011) 79–101.